Two-Stage Aerosol Synthesis of Titanium Nitride TiN and Titanium Oxynitride TiO_xN_y Nanopowders of Spherical Particle Morphology

Mariusz Drygaś,[†] Cezary Czosnek,[†] Robert T. Paine,[‡] and Jerzy F. Janik*,[†]

Faculty of Fuels and Energy, AGH University of Science and Technology, Al. Mickiewicza 30, 30-059 Kraków, Poland, and Department of Chemistry, University of New Mexico, Albuquerque, New Mexico 87131

Received March 3, 2006

The two-stage aerosol-assisted synthesis technique was first used to prepare titanium containing raw aerosol powders with spherical particle morphology from aqueous and methanol solutions of selected oxygen-bearing titanium precursors and from neat titanium(IV) *i*-propoxide. The aerosol powders were subsequently pyrolyzed under ammonia at 1000, 1100, and 1200 °C, giving, in some favorable cases, compositions ranging from titanium oxynitride TiO_xN_y to titanium nitride TiN with average crystallite sizes of 32−38 nm and a residual oxygen content in the latter below 2 wt %. The intermediate and final products were characterized by SEM, XRD, FT-IR, and XPS analytical methods. For selected materials, oxygen content, helium density, and BET surface area were also determined.

1. Introduction

Titanium nitride TiN is an important technological material with diverse applications that are derived from its unique properties. It has a hardness of 2160 kG/mm^2 nearing that of diamond and a high melting point around 3000 °C; it also shows significant chemical corrosion resistance.[1] Other important properties include electric conductivity that is higher than that of titanium metal and low-temperature superconductivity.[2] Light-absorption properties of TiN are utilized in manufacturing screens with adjustable light transmission, and TiN is used in microelectronic VLSI devices as a highly conductive diffusion barrier. The potential for making Shottky diodes and MOS transistor gates has also been proposed.[3] In related areas, the resistivity of thin films of TiO_xN_y can be adjusted by regulating the *x* parameter,[4] and the oxynitride's structural and chemical compatibility with TiN are advantageous for a new generation of nonvolatile memory (PCRAM) structures.[5]

There are several methods quoted in the literature for the preparation of TiN. They include the conventional methods of nitridation of Ti−metal (or titanium hydride) with various nitrogen sources,[6] carbothermal reduction/nitridation of TiO_2,[7] and chemical vapor deposition utilizing volatile precursors such as $TiCl_4$ and $Ti(NR_2)_4$ (R═CH_3, C_2H_5) and ammonia.[2,8] These approaches typically produce microcrystalline TiN because of the high temperatures required for completing the nitridation reactions, especially when oxygen-containing precursors are employed. There are a few reports of the preparation of nanocrystalline powders of titanium nitride that include a laser ablation method,[9a] direct ammonolysis of $TiCl_4$,[9b] hydrolysis/ammonolysis of $TiCl_4$ and $Ti(O-i-C_3H_7)_3$,[9c] direct nitridation of nano-TiO_2,[9d] and metathesis of $TiCl_4$ with NaN_3[9e] or $NaNH_2$.[1]

Commercially available titanium oxygen compounds offer affordable sources for titanium nitride nanopowders. However, there exist thermodynamic and kinetic barriers to replacement of the strong Ti−O bonds with Ti−N bonds through diffusion-controlled reactions within solid-state particles that must occur at low temperatures that suppress crystal growth/recrystallization phenomena. This situation is complicated by the existence of stable titanium oxynitride TiO_xN_y compositions, both in thin films[5,10] and bulk solids,[11] that can be thought of as solid solutions of cubic TiN (a =

* Corresponding author. E-mail: janikj@agh.edu.pl.
[†] AGH University of Science and Technology.
[‡] University of New Mexico.

(1) Chen, L.; Gu, Y.; Shi, L.; Ma, J.; Yang, Z.; Qian, Y. *J. Nanosci. Nanotechnol.* **2004**, *4*, 896.
(2) Fix, R. M.; Gordon, R. G.; Hoffman, D. M. *Chem. Mater.* **1990**, *2*, 235.
(3) Fix, R.; Gordon, R. G.; Hoffman, D. M. *Chem. Mater.* **1991**, *3*, 1138.
(4) Martin, N.; Banakh, O.; Santo, A. M. E.; Springer, S.; Sanjinés, R.; Takadoum, J.; Lévy, F. *Appl. Surf. Sci.* **2001**, *185*, 123.
(5) Kang, D.-H.; Ahn, D.-H.; Kwon, M.-H.; Kwon, H.-S.; Kim, K.-B.; Lee, K.-S.; Cheong, B.-K. *Jpn. J. Appl. Phys.* **2004**, *43*, 5243.
(6) (a) Toth, L. *Transition Metal Carbides and Nitrides*; Academic Press: New York, 1971. (b) Hwang, Y.-H.; Un, C.-I. *J. Chem. Eng. Jpn.* **1998**, *31*, 214. (c) Zhu, L.; Ohashi, M.; Yamanaka, S. *Mater. Res. Bull.* **2002**, *37*, 475.
(7) (a) Ortega, A.; Roldan, M. A.; Real, C. *Int. J. Chem. Kinet.* **2005**, *37*, 566. (b) Peelamedu, R. D.; Fleming, M.; Agrawal, D. K.; Roy, R. *J. Am. Ceram. Soc.* **2002**, *85*, 117. (c) Vaidhyanathan, B.; Rao, K. J. *Chem. Mater.* **1997**, *9*, 1196. (d) White, G. V.; Mackenzie, K. J. D.; Brown, I. W. M.; Bowden, M. E.; Johnston, J. H. *J. Mater. Sci.* **1992**, *27*, 4287.
(8) Truong, C. M.; Chen, P. J.; Corneille, J. S.; Oh, W. S.; Goodman, D. W. *J. Phys. Chem.* **1995**, *99*, 8831.
(9) (a) Reinholdt, A.; Pecenka, R.; Pinchuk, A.; Runte, S.; Stepanov, A. L.; Weirich, T. E.; Kreibig, U. *Eur. Phys. J. D* **2004**, *31*, 69. (b) Kaskel, S.; Schlichte, K.; Chaplais, G.; Khanna, M. *J. Mater. Chem.* **2003**, *13*, 1496. (c) Kawano, S.; Takahashi, J.; Shimada, S. *J. Am. Ceram. Soc.* **2003**, *86*, 1609. (d) Li, J.; Gao, L.; Sun, J.; Zhang, Q.; Guo, J.; Yan, D. *J. Am. Ceram. Soc.* **2001**, *84*, 3045. (e) Hu, J.; Lu, Q.; Tang, K.; Yu, S.; Qian, Y.; Zhou, G.; Liu, X. *J. Am. Ceram. Soc.* **2000**, *83*, 430.
(10) For example, see (and references therein): (a) Martev, I. N. *Vacuum* **2002**, *67*, 261. (b) Vaz, F.; Cerqueira, P.; Rebouta, L.; Nascimento, S. M. C.; Alves, E.; Goudeau, P.; Rivière, J. P.; Pischow, K.; de Rijk, J. *Thin Solid Films* **2004**, *447−448*, 449.
(11) Yang, X.; Li, C.; Yang, B.; Wang, W.; Qian, Y. *Chem. Phys. Lett.* **2004**, *383*, 502.

10.1021/cm060522z CCC: $33.50
Published on Web 05/27/2006

4.241 Å) and disordered cubic TiO ($a = 4.173$ Å). In this regard, there are known two TiO oxides with the nominal Ti^{2+} oxidation state. These are the nonstoichiometric disordered TiO having a heavily defected lattice with systematic and random absences of cubic symmetry[12,13] and the stoichiometric ordered TiO with structural vacancies in metallic and nonmetallic sublattices reported to be monoclinic.[12c]

Herein is reported the application of a two-stage aerosol-assisted synthesis method for the preparation of TiN or TiO_xN_y bulk powders from affordable titanium precursors. The method has already been successfully used in our laboratories to make nanosized powders of the nitrides BN[14] and GaN[15] as well as composites in the systems GaN/TiN[16] and GaN/Mn.[17] In the first stage, complex decomposition and partial nitridation reactions take place during the aerosol generation between ammonia and submicrometer-sized droplets containing a precursor and solvent (water or methanol). The bulk aerosol powders obtained from this processing are usually subjected to a second-stage pyrolysis under ammonia to complete nitridation of products that have spheroidal particle morphology. We point out that one of the outstanding features of the aerosol-assisted process is that all reactions take place within very small liquid and solid particles suspended in a reactive gas stream. In favorable cases, this creates more-advantageous conditions for nitridation toward nanosized particles compared to typical one-stage bulk pyrolysis methods.

2. Experimental Section

Aqueous and methanol solutions of selected titanium precursors as well as neat $Ti(O-i-C_3H_7)_4$ were used in an aerosol generator and under conditions described elsewhere.[14−17]

Aqueous Solutions. Transparent aqueous solutions of titanium(IV) chloride $TiCl_4$ (0.1 M) were prepared by slow addition of neat chloride (0.05 mol, 5.5 cm^3) to stirred DI water (495 cm^3) at 0 °C.[18] Similar transparent solutions of 0.1 M $Ti(NO_3)_4$ were synthesized in situ according to a published procedure.[18] All solutions were prepared immediately before aerosol generation. Aerosol formation was accomplished as described previously.[14−17] The mullite reactor tube was held at 1000 °C and gas-flow rates were 1 L/min for N_2 and 3 L/min for NH_3 for $Ti(NO_3)_4$ solutions or 4 L/min for $TiCl_4$ solutions. The second-stage bulk powder pyrolyses were accomplished in an alumina boat at 1000, 1100, and 1200 °C for 6 h under a NH_3 flow of 0.5 L/min. Products were dark brown to black free-flowing powders.

Methanol Solutions. The liquid $Ti(OCH_3)_4$, $Ti(OC_2H_5)_4$, and $Ti(O-i-C_3H_7)_4$ were individually added dropwise at 23 °C to an appropriate amount of methanol to yield 0.1 M solutions. Initially, white precipitates/suspensions formed; however, additions of 1.5 mL of concentrated HNO_3 per 1000 mL of solution, with stirring for several hours, gave transparent, stable colloidal solutions. Aerosol generation was performed as described above. Subsequent pyrolyses were carried out under conditions identical to those above. Products were dark gray (1000 °C) to dark brown (1100 and 1200 °C) powders.

Neat Titanium(IV) *i*-propoxide $Ti(O-i-C_3H_7)_4$. The surface tension of neat $Ti(O-i-C_3H_7)_4$ retards aerosol generation at ambient temperatures; therefore, aerosols were generated with a water bath (80−90 °C) surrounding the sample container. About 40 mL of liquid were consumed during an 8 h run, affording 6.2 g of a black powder. Subsequent pyrolyses of this powder under conditions identical to those above gave dark brown powders.

Reference TiO_2 and TiO Powders. Two commercially available titanium oxide powders (Aldrich), i.e., white TiO_2 (anatase; average crystallite size, 116 nm; BET surface area, 6.5 m^2/g) and brown TiO (stoichiometric, monoclinic) were nitrided/pyrolyzed in an alumina boat as described above.

All products were characterized by powder XRD (Siemens D5000 with Cu K_α source; $2\theta = 20-80°$; average crystallite sizes were calculated from Scherrer's equation,[19] $D(\text{diameter}) = 0.9\,\lambda/(d \cos \Theta)$), FT-IR (KBr pellets; Bruker Tensor 27), SEM (platinum coating; Hitachi-S800), and XPS (Vacuum Systems Workshop Ltd., Al K_α X-ray source, energies referenced vs carbon, 284.6 eV). For selected samples, helium densities (Micromeritics AccuPyc), BET surface areas (Micromeritics Gemini 2360), and oxygen analyses (Saint-Gobain Advanced Ceramics Corp., Amherst, NY) were also determined.

3. Results and Discussion

The chemistry involved in conversion of the selected titanium precursors to titanium nitride is thought to include, initially, the thermal decomposition of the inorganic or alkoxide precursors that are all known to yield titanium oxide TiO_2 at moderately high temperatures.[20] This intermediate is expected to react in situ with ammonia at sufficiently high temperatures to produce c-TiN. However, there is ample evidence that such a conversion in oxygen-bearing precursor systems involves the formation of stable titanium oxynitrides, c-TiO_xN_y, of variable composition.[5,9,11] In the case of alkoxy derivatives, the presence of carbon and/or carbon monoxide from thermal cracking of the alkoxy groups may positively enhance the rate of conversion of oxide to nitride via the known carbothermal reduction/nitridation mechanism.[7]

It is known that two of the $Ti(OR)_4$ precursors (R═C_2H_5, i-C_3H_7) in methanol produce transesterification chemistry with the formation/precipitation of the methoxy derivative according to the idealized equation $Ti(OR)_4 + 4CH_3OH = Ti(OCH_3)_4 + 4ROH$.[21] Therefore, the $Ti(OC_2H_5)_4$/methanol and $Ti(O-i-C_3H_7)_4$/methanol systems are chemically similar to the $Ti(OCH_3)_4$/methanol system. It is also thought that dissolution in methanol of the essentially methanol-insoluble

(12) (a) Watanabe, D.; Castles, J. R.; Jostsons, A.; Malin, A. S. *Acta Crystallogr.* **1967**, *23*, 307. (b) Waldner, P.; Eriksson, G. *CALPHAD* **1999**, *23*, 189. (c) Valeeva, A. A.; Gusev, A. I. *JETP Lett.* **2004**, *79*, 468.
(13) Banakh, O.; Schmid, P. E.; Sanjinés, R.; Lévy, F. *Surf. Coat. Technol.* **2002**, *151−152*, 272.
(14) (a) Pruss, E. A.; Wood, G. L.; Kroenke, W. J.; Paine, R. T. *Chem. Mater.* **2000**, *12*, 19. (b) Paine, R. T.; Kroenke, W. J.; Pruss, E. A.; Wood, G. L.; Janik, J. F. U.S. patent 6 824 753, Sept 30, 2004.
(15) (a) Wood, G. L.; Pruss, E. A.; Paine, R. T. *Chem. Mater.* **2001**, *13*, 12. (b) Janik, J. F.; Drygaś, M.; Stelmakh, S.; Grzanka, E.; Pałosz, B.; Paine, R. T. *Phys. Status Solidi A* **2006**, *203*, 1301.
(16) Drygaś, M.; Czosnek, C.; Paine, R. T.; Janik, J. F. *Mater. Res. Bull.* **2005**, *40*, 1136.
(17) Janik, J. F.; Drygaś, M.; Czosnek, C.; Kamińska, M.; Palczewska, M.; Paine, R. T. *J. Phys. Chem. Solids* **2004**, *65*, 639.
(18) Jung, C. H.; Park, J. Y.; Oh, S. J.; Park, H. K.; Kim, Y. S.; Kim, D. K.; Kim, J. H. *J. Nucl. Mater.* **1998**, *253*, 203.
(19) Klug, H. P.; Alexander, L. E. *X-ray Diffraction Procedures*; Wiley: New York, 1974.
(20) (a) Zheng, Y.; Shi, E.; Cui, S.; Li, W.; Hu, X. *J. Am. Ceram. Soc.* **2000**, *83*, 2634. (b) Kim, H.-S.; Campbell, S. A.; Gilmer, D. C.; Kaushik, V.;Conner, J.; Prabhu, L.; Anderson, A. *J. Appl. Phys.* **1999**, *85*, 3278 and references therein.
(21) Campbell, C.; Bott, S. G.; Larsen, R.; Vandersluys, W. G. *Inorg. Chem.* **1994**, *33*, 4950 and references therein.

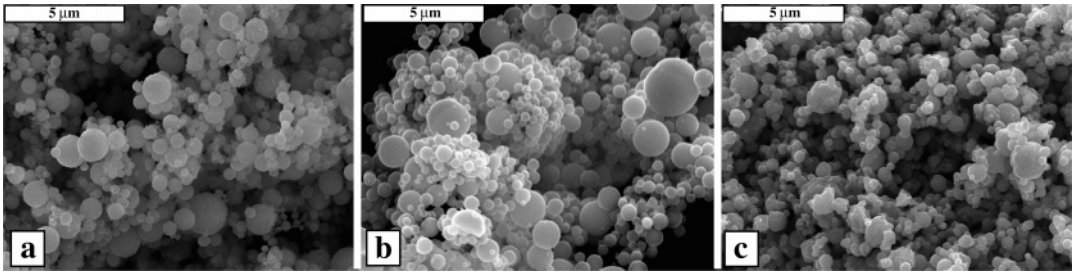

Figure 1. SEM images for: (a) aerosol powder formed at 1000 °C from the $Ti(NO_3)_4/H_2O/NH_3$ system; (b) powder after second-stage pyrolysis at 1100 °C from the $Ti(NO_3)_4/H_2O/NH_3$ system; and (c) powder after second-stage pyrolysis at 1100 °C from the $TiCl_4/H_2O/NH_3$ system.

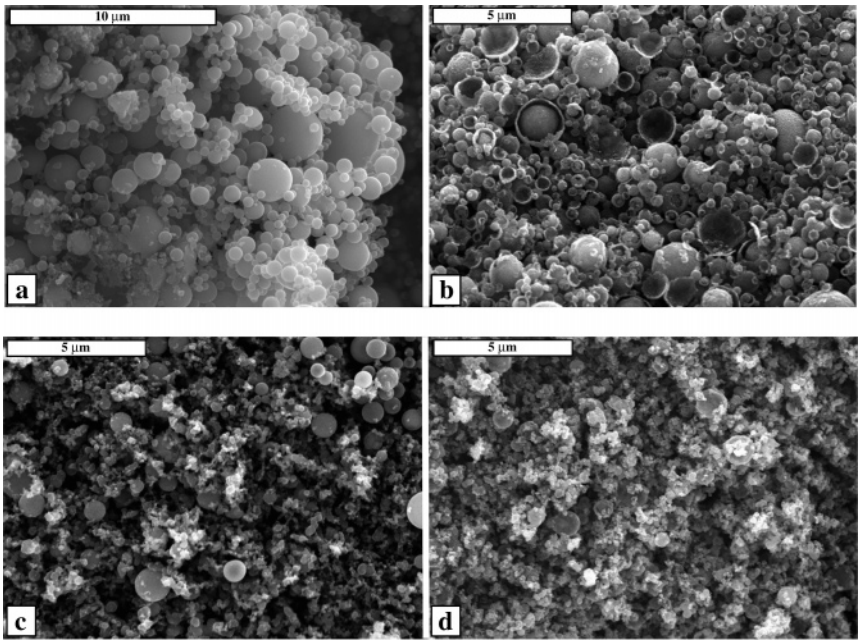

Figure 2. SEM images for: (a) aerosol powder formed at 1000 °C from the $Ti(OCH_3)_4/CH_3OH/NH_3$ system; (b) powder after second-stage pyrolysis at 1100 °C from the $Ti(OCH_3)_4/CH_3OH/NH_3$ system; (c) aerosol powder formed at 1000 °C from neat $Ti(O-i\text{-}C_3H_7)_4/NH_3$; and (d) powder after second-stage pyrolysis at 1100 °C from neat $Ti(O-i\text{-}C_3H_7)_4/NH_3$.

titanium(IV) methoxide upon addition of a small amount of concentrated nitric acid is associated with peptization and formation of an acid-stabilized colloid.[22]

On the basis of our experience with the synthesis of a variety of nitride nanopowders and the severe problems associated with elemental analysis for such materials,[14−17] we believe that an O content level below approximately 2 wt % is mainly associated with the presence of surface oxides on otherwise phase-pure nitride particles. For samples with higher O content levels, we might theoretically calculate the *x* and *y* coefficients in the oxynitride formula on the basis of the electroneutrality principle. However, we find no clear literature delineation of the nature of the titanium oxynitride powder composition/structure condition, i.e., stoichiometric vs defect type compound. Given the possible existence of defected structures and recognizing the controversy surrounding the quantitative interpretation of XRD data for nanocrystalline powders, we are handicapped with the application of Vegard's law that otherwise could help us estimate the coefficients. Eventually, our criterion for the cubic phase materials is that those with an O content in the 2 wt % and below range are assumed to be pure TiN, whereas others with a higher O content level are considered oxynitrides, which is positively corroborated by the relevant XRD, FT-IR, XPS, and density data.

3.1. SEM Examination. *(a) Aqueous Solution Systems.* The aerosol powders formed at 1000 °C from these systems show a well-defined spherical morphology that is mostly preserved following the additional bulk powder pyrolysis (Figure 1). The powders from the system $TiCl_4/H_2O/NH_3$ are spherical but appear to be slightly deformed (Figure 1c). The particles are only slightly agglomerated, with sizes ranging from a few tenths to 2−3 micrometers.

(b) Methanol Solution and Neat $Ti(O-i\text{-}C_3H_7)_4$ Systems. The aerosol powders formed at 1000 °C from methanol solutions of $Ti(OR)_4$ also display spherical morphology (Figure 2a,b). The particle dimensions are similar to those for the powders derived from the aqueous solutions. However, in this case, the pyrolyzed powders contain numerous empty-shell fragments. Note that the shattered shells are likely an artifact of sample preparation for SEM examination. The AAVS process appears to produce mostly empty-shelled spheres, similar to the reported anaerobic synthesis of TiN from $TiCl_4$ and $NaNH_2$.[1]

In contrast to the above, the aerosol powder from the neat $Ti(O-i\text{-}C_3H_7)_4/NH_3$ system contains a mixture of spheres and abundant, irregularly shaped particles. On the basis of

(22) Vorkapic, D.; Matsoukas, T. *J. Am. Ceram. Soc.* **1998**, *81*, 2815.

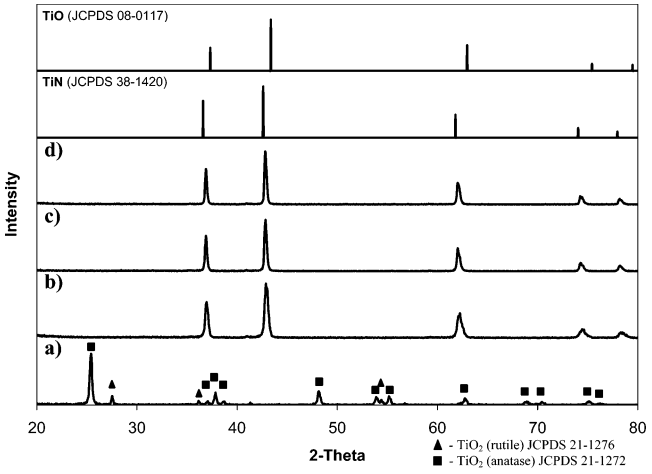

Figure 3. XRD patterns for products from (a) the aerosol powder obtained at 1000 °C from the $Ti(NO_3)_4/H_2O/NH_3$ system and powders after second-stage pyrolysis at (b) 1000, (c) 1100, and (d) 1200 °C.

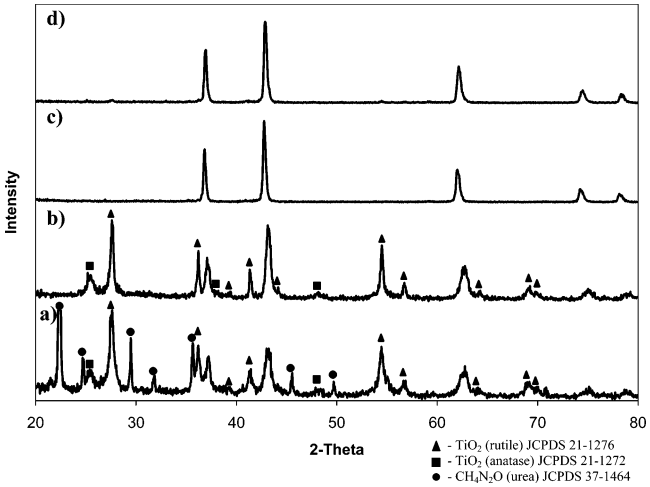

Figure 4. XRD patterns for products from (a) aerosol powder formed at 1000 °C from the $Ti(OCH_3)_4/CH_3OH/NH_3$ system and powders after second-stage pyrolysis at (b) 1000, (c) 1100, and (d) 1200 °C.

the information available at this time, it is not clear whether the irregular fines are a result of aerosol particle bursting events or, perhaps, competing CVD-like conversion chemistry between the vapors of $Ti(O-i-C_3H_7)_4$ and NH_3 (Figure 2c). Such irregular morphology is then retained in the powders produced from the second-stage pyrolysis (Figure 2d).

3.2. Powder XRD Results. *(a) Aqueous Solution Systems.* Figure 3 shows XRD scans for powders prepared in the aerosol system $Ti(NO_3)_4/H_2O/NH_3$ and, subsequently, bulk pyrolyzed under an ammonia atmosphere at 1000, 1100, and 1200 °C. Additionally, JCPDS reference XRD scans for cubic TiN and cubic TiO are included.

On the basis of the XRD pattern for the aerosol formed at 1000 °C, the raw powder is largely composed of anatase and rather small amounts of rutile, the ambient and high-temperature phases of TiO_2, respectively (Figure 3a). This indicates that little nitridation apparently occurs during the aerosol generation stage, because of relatively short particle residence times in the hot reaction zone. All XRD patterns obtained for the pyrolyzed products under NH_3 correspond to a single cubic phase. The patterns' features range from the 1000 °C product with peaks relatively close to the reference pattern for cubic titanium monoxide, c-TiO (JCPDS 08-0117), to the 1200 °C product corresponding very closely to the pattern for cubic titanium nitride, c-TiN (JCPDS 38-1420). Regardless of the pyrolysis temperature, there are no indications of the existence of any plausible TiO_2 phases, i.e., rutile and anatase, or lower titanium oxides. It follows that the applied pyrolysis conditions are efficient in conversion of the intermediate nano-TiO_2 phases toward the nitrided materials. The XRD patterns for the corresponding products from the $TiCl_4/H_2O/NH_3$ system (not shown here) are very similar to the ones just discussed. On the basis of peak positions and peak widths, crystallographic cell parameters for the cubic phase and average crystallite sizes were calculated and included in Table 1.

In all cases, the *a* values are somewhat less than the 4.241 Å observed for microcrystalline c-TiN and much greater than the 4.173 Å found for microcrystalline c-TiO. The intermediate values are consistent with the formation of cubic titanium oxynitride and the gradual replacement of O atoms with N atoms in products obtained at increased temperatures.[5,10−12,20] It is apparent that with increased pyrolysis temperatures, the lattice constants in both systems closely approach the limiting cell parameter for c-TiN. The average crystallite size spans 26−43 nm and increases with increasing pyrolysis temperature. The change in crystallite size suggests that grain growth is most affected between 1000 and 1100 °C.

Table 1. Crystallographic Cell Parameters for the Cubic Phase and Average Crystallite Sizes for Pyrolyzed Products in the Aqueous Aerosol Systems

pyrolysis temperature (°C)	cubic phase cell parameter *a* (Å)	average crystallite size *d* (nm)
	$Ti(NO_3)_4/H_2O/NH_3$	
1000	4.227	26
1100	4.230	40
1200	4.236	43
	$TiCl_4/H_2O/NH_3$	
1000	4.222	29
1100	4.230	38
1200	4.232	37

(b) Methanol-Based Solution and Neat $Ti(O-i-C_3H_7)_4$ Systems. As a representative example for the methanol-based systems, Figure 4 presents the XRD patterns obtained for the aerosol powder formed at 1000 °C and for the pyrolyzed products from the solution system $Ti(OCH_3)_4/CH_3OH/NH_3$. The XRD scan for the raw aerosol powder can be indexed to include the prevailing rutile phase and minor anatase phase of TiO_2, with the trend in these phases' amounts being opposite to that in the aqueous system $Ti(NO_3)_4/H_2O/NH_3$ discussed previously. There is also a significant amount of cubic phase, with characteristics close to those of titanium oxynitride with small amounts of nitrogen. Additionally, there is a fourth component in the mixture, namely urea, which is commonly observed in raw aerosol powders from the AAVS process when methanol is employed as solvent. This compound is always absent in the subsequently pyrolyzed powders, mainly because of its high volatility and thermal decomposition under processing conditions.[23]

(23) (a) Podsiadło, S. *Thermochim. Acta* **1995**, *256*, 367. (b) Qiu, Y.; Gao, L. *J. Am. Ceram. Soc.* **2004**, *87*, 352.

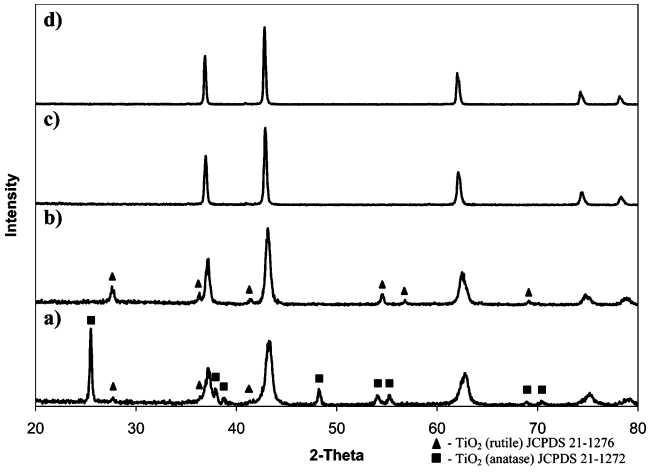

Figure 5. XRD patterns for products from (a) aerosol powder formed at 1000 °C from neat $Ti(O-i-C_3H_7)_4/NH_3$ and powders after pyrolysis at (b) 1000, (c) 1100, and (d) 1200 °C.

The dominant crystallographic phase in all three second-stage pyrolyzed products has a cubic symmetry pattern that is placed somewhere between those for c-TiN and c-TiO. The temperature-dependent trend of the cubic pattern observed here is also similar to the data discussed for the aqueous solution systems. However, in this case, there is also a difference between these solvent systems in that the XRD pattern for the 1000 °C powder contains, in addition to the cubic phase, strong peaks assigned to rutile (major) and anatase (minor). It is interesting to note that the relative proportions of all three Ti-containing phases are very similar to their amounts in the aerosol powder before pyrolysis when disregarding the urea component (Figure 4a,b). This observation is consistent with a low degree of nitridation at 1000 °C. Despite an improved nitridation during aerosol generation in the methanol-based systems vs the aqueous systems, supported by the presence of the cubic phase in the aerosol powder of the former, the concurrent preferred crystal growth of TiO_2, especially rutile, negatively impacts the reactivity of the powder toward further nitridation at 1000 °C. In this regard, the improved first-stage nitridation may be a manifestation of the carbothermal reduction/nitridation mechanism playing a positive role under the conditions of aerosol generation but not operating during the subsequent 1000 °C pyrolysis of bulk powders. However, the application of the higher pyrolysis temperatures up to 1200 °C results in continuing nitridation of the aerosol and the formation of TiN.

Figure 5 shows the XRD data collected for pyrolyzed products obtained from the neat $Ti(O-i-C_3H_7)_4/NH_3$ aerosol system. The raw aerosol powder is composed of the major cubic phase with pattern characteristics corresponding to those of titanium oxynitride with a low nitrogen content and the anatase and minor rutile phases of TiO_2. Interestingly, anatase is the major phase in this system, compared with rutile being found as the main oxide phase in the system $Ti(OCH_3)_4/CH_3OH/NH_3$. The carbothermal reduction/nitridation is also quite effective in this system (efficient cubic-phase formation), whereas the simultaneous crystal growth of TiO_2 occurs toward anatase. The nitriding pyrolysis of this aerosol at 1000 °C results in a major cubic phase and a small amount of rutile, supporting an overall more-advantageous nitridation compared to the related methanol solvent system products. By comparing the effects of the pyrolysis at 1000 °C in both alkoxide systems, it appears that anatase is more reactive toward nitridation than rutile, the latter constituting a significant barrier at this temperature. The XRD patterns for the 1100 and 1200 °C pyrolyzed materials show the cubic phase exclusively, indicating again that the conversion of both TiO_2 phases is completed in this temperature range. The crystallographic parameters calculated from the patterns are included in Table 2. In general, the cubic cell parameters increase and approach the limiting value for c-TiN with increasing pyrolysis temperatures, especially up to 1100 °C. The range of crystallite sizes, 20−42 nm, and, especially above 1100 °C, i.e., 29−42 nm, is similar to the values found in the aqueous systems (see Table 1). The changes both in cell parameters and average crystallite sizes tend to level off after 1100 °C; in a few cases, slightly lower values of these parameters are observed in materials after the 1200 °C pyrolysis. This trend is qualitatively similar in both solvent systems and indicates that the most-dynamic nitridation occurs up to 1100 °C. Interestingly, when comparing the cubic cell dimensions for these alkoxy systems with the aqueous-based inorganic systems after the 1000 °C pyrolysis, the significantly lower *a* values in the former support a lower degree of nitridation and relatively more oxygen in the oxynitrides. This observation agrees with the presence of rutile in the low-temperature products, which generally signals poorer nitridation circumstances. However, the pyrolyses at 1100 °C and above appear to yield similarly good nitridation effects in both solvent systems.

(c) TiO_2/NH_3 and TiO/NH_3 Reference Precursor Systems. Commercial TiO_2 (anatase) and TiO (monoclinic) were pyrolyzed as bulk powders under an ammonia flow under similar conditions as those in the systems described above. Table 3 includes the relevant crystallographic data extracted from the relevant XRD patterns (not shown). A detailed analysis of the patterns suggests that the nitridation of TiO appears to be more feasible than nitridation of TiO_2 under comparable conditions. In the former case, the exclusive cubic phase of titanium oxynitride is confirmed already after the 1000 °C pyrolysis, whereas in the latter, there are significant quantities of TiO_2, especially rutile, still present in the related 1000 °C product. Rutile is even detected in small amounts in the 1200 °C product. This is consistent with the previously discussed cases, in which rutile was found to be the least reactive toward nitridation among the encountered titanium oxide phases. In addition, the cell parameters of the cubic phase in the comparable products from nitridation of TiO are larger and indicative of higher proportions of nitrogen in the transient oxynitride compared with the nitridation of TiO_2 (Table 3).

3.3. FT-IR Study. In the FT-IR spectra (not shown) obtained for products pyrolyzed at 1000 °C, there is a broad band at 540−640 cm^{-1} that is characteristic of Ti−O absorptions in titanium oxides.[24] TiN has no absorption bands above 400 cm^{-1}. At increased pyrolysis temperatures, the Ti−O bands are barely visible for the 1100 °C products and

(24) Ariya, S. M.; Golomolzina, V. *Zh. Obshch. Khim.* **1963**, *33*, 1389.

Table 2. Crystallographic Cell Parameters for the Cubic Phase and Average Crystallite Sizes for Pyrolyzed Products in Methanol-Based and Neat $Ti(O-i-C_3H_7)_4$ Aerosol Systems

pyrolysis temperature (°C)	cubic phase cell parameter *a* (Å)	average crystallite size *d* (nm)	pyrolysis temperature (°C)	cubic phase cell parameter *a* (Å)	average crystallite size *d* (nm)
	$Ti(OCH_3)_4/CH_3OH/NH_3$			$Ti(O-i-C_3H_7)_4/CH_3OH/NH_3$	
1000	4.201	26	1000	4.195	20
1100	4.235	32	1100	4.228	34
1200	4.228	29	1200	4.231	30
	$Ti(OC_2H_5)_4/CH_3OH/NH_3$			Neat $Ti(O-i-C_3H_7)_4/NH_3$	
1000	4.205	22	1000	4.197	20
1100	4.233	35	1100	4.233	33
1200	4.225	35	1200	4.235	42

Table 3. Crystallographic Cell Parameters for the Cubic Phase and Average Crystallite Sizes for Pyrolyzed Products in the Reference Precursor Systems TiO_2/NH_3 and TiO/NH_3

pyrolysis temperature (°C)	cubic phase cell parameter *a* (Å)	average crystallite size *d* (nm)
	TiO_2/NH_3	
1000	4.194	26
1100	sn/a[a]	sn/a[a]
1200	4.223	36
	TiO/NH3	
1000	4.224	22
1100	4.230	32
1200	4.233	33

[a] sn/a = sample not available.

nondetectable for the 1200 °C products; the latter, therefore, contain only minimal quantities of Ti−O below the detection limits of the method.

3.4. XPS Study. Figures 6 and 7 show the Ti 2p and N 1s bands for the 1100 °C products from the aqueous system $Ti(NO_3)_4/H_2O/NH_3$ and methanol system $Ti(OCH_3)_4/CH_3OH/NH_3$, respectively, which are representative for other materials in this study. The major N 1s peak at 396.5 eV is typical for nitrogen shifts in metal nitrides and oxynitrides.[25] The smaller intensity N 1s peak at 399.9 eV is in the range proposed for terminally bound nitrogen that is released during nitridation of Ti−O sites or in surface oxynitrides.[25d] The deconvolution of the complex Ti 2p bands yields in each case three major doublets ($2p_{3/2}$ and $2p_{1/2}$) encompassing the set of three $2p_{3/2}$ peaks, namely, at 455.1 eV typical for TiN, at 456.7 eV in the range for TiO or TiO_xN_y, and at 458.2 eV for TiO_2.[25] The lower-intensity peaks at approximately 470 and 476 eV are plasmon lines, and peaks at approximately 450 eV are due to unfiltered $K_{\alpha 2}$ and $K_{\alpha 3}$ bands.

These results are consistent with the XRD patterns in that both methods provide specific evidence for the occurrence of titanium oxynitride and/or TiN domains. In this regard, phase-detection limits of XRD measurements are close to a few weight percent, and small quantities of crystalline TiO_2 will go undetected by XRD. On the other hand, XPS spectroscopy is oversensitive to surface groups; it is known that particles of titanium nitride and titanium oxynitride are very prone to surface passivation with atmospheric oxygen, leading to amorphous TiO_2[26] and relative enhancement of the peak at 458.2 eV. It is evident from Figures 6 and 7 that the Ti 2p peaks vary in relative intensities in the two products. Such variations are commonly observed also in the XPS spectra for other investigated materials in this study (not shown here) and can be traced to the samples' surface properties and preparation history. Therefore, because of the facile surface oxidation of nitrided particles, the XPS spectroscopy fails to provide solid evidence for an unreacted primary TiO_2. However, these results prove that both the titanium oxynitride and TiN domains are present. This is an important observation because it provides evidence that the nitridation conversion of the powders under the applied conditions will eventually yield TiN with, possibly, some titanium oxynitride and not only a single oxynitride phase with varying oxygen content.

Figure 8 displays the Ti 2p and N 1s deconvoluted bands for the 1000 °C product from the previously discussed system $Ti(OCH_3)_4/CH_3OH/NH_3$. Interestingly, no unequivocal strong Ti 2p peaks due to titanium nitride TiN are found; the two major peaks are typical for the TiO_2 and TiO_xN_y chemical environments. This suggests that there may be only scarce TiN domains. In this regard, the relevant XRD spectrum for this material (Figure 4a) suggests in a coherent way the presence of a mixture of crystalline TiO_2 and TiO_xN_y. The strongest Ti $2p_{3/2}$ peak at 458.6 eV typical for TiO_2 can thus be linked to some unreacted TiO_2. The corresponding N 1s band is consistent with this picture, with the major peak at 395.8 eV due to nitrogen in the bulk oxynitride and the smallest peak at 398.0 eV linked to the adsorbed nitrogen that is released during nitridation of Ti−O sites or to surface oxynitride species.[25d] The medium-sized peak at 401.7 eV is in the range for organically bound nitrogen and may indicate some residual contaminant N≡C species. It is worth mentioning that prolonged ion sputtering of TiN films that initially show a N 1s chemical environment in the 398−400 eV range results in removal of the peak attributable to this species, indicating their surface origin.[25d] The characteristics of the relevant O 1s and C 1s bands (not shown) are in qualitative agreement with the above conclusions. Particularly, there are no C 1s peaks that would indicate structural incorporation of carbon by forming titanium−carbon bonds.

3.5. Oxygen Content, Helium Density, and BET Surface-Area Data. The bulk powder oxygen content (O content) in the materials primarily reflects the extent of nitridation; for the high-temperature-derived products with small residual O content, it will also include a significant contribution from the secondary TiO_2 because of particle surface oxidation. From Table 4, it is clear that the lowest O content levels are found in the powders from the aqueous solution systems at

(25) (a) Biwer, B. M.; Bernasek, S. L. *Surf. Sci.* **1986**, *167*, 207. (b) Ahn, Y. S.; Ban, S. H.; Kim, K. J.; Kang, H.; Yang, S.; Roh, Y.; Lee, N.-E. *Jpn. J. Appl. Phys.* **2002**, *41*, 7282. (c) Lu, F.-H.; Chen, H.-Y. *Thin Solid Films* **1999**, *355*−*356*, 374. (d) Jiang, N.; Zhang, H. J.; Bao, S. N.; Shen, Y. G.; Zhou, Z. F. *Physica B* **2004**, *352*, 118.
(26) Tompkins, H. G. *J. Appl. Phys.* **1991**, *70*, 3876.

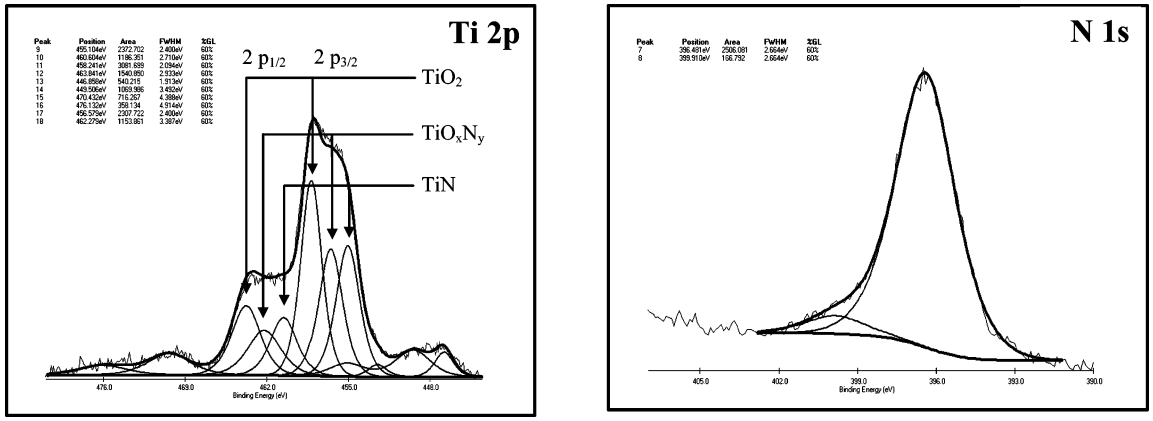

Figure 6. XPS spectra for product from the system $Ti(NO_3)_4/H_2O/NH_3$ after pyrolysis at 1100 °C.

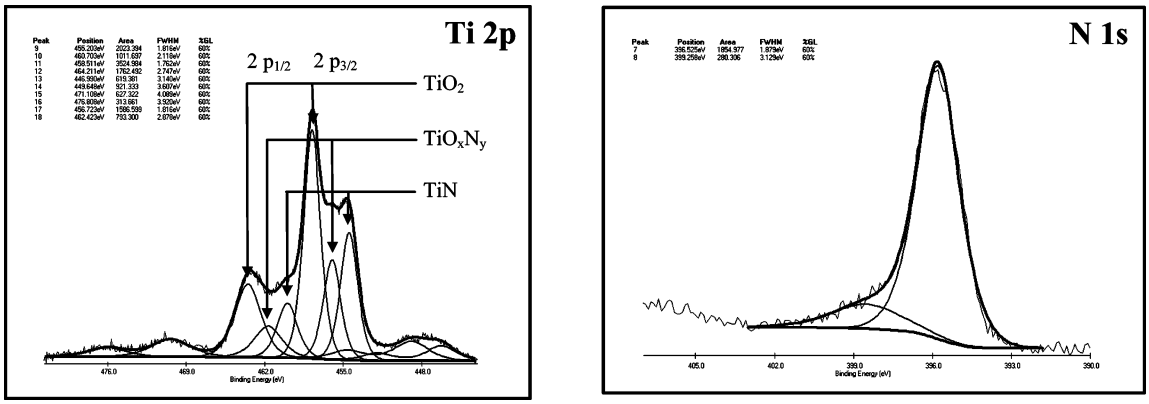

Figure 7. XPS spectra for product from the system $Ti(OCH_3)_4/CH_3OH/NH_3$ after pyrolysis at 1100 °C.

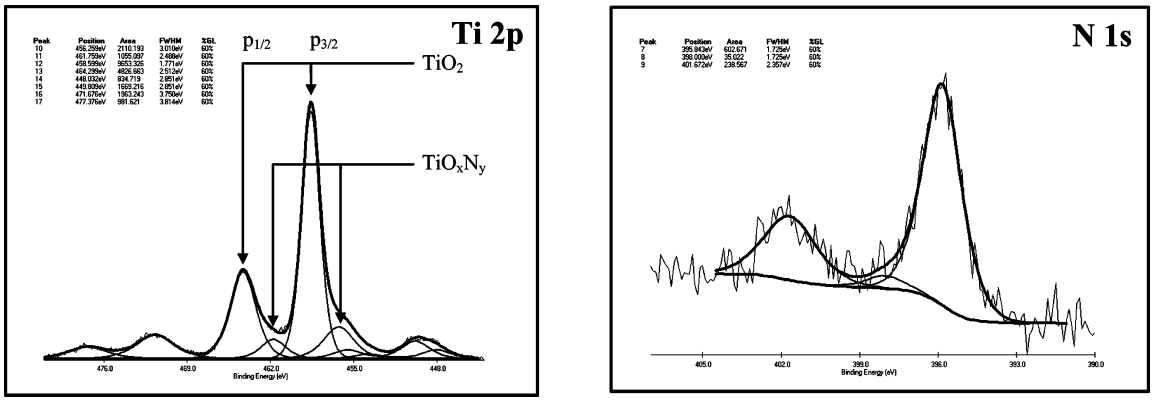

Figure 8. XPS spectra for product from the system $Ti(OCH_3)_4/CH_3OH/NH_3$ after pyrolysis at 1000 °C.

all pyrolysis temperatures. For instance, the O content levels in the 1000 °C powders from such systems are in the range 3.5−7.8 wt %, compared with the range 20.5−23.7 wt % in the titanium alkoxide/methanol-based systems. It is interesting to compare these values with the O content analyzed in the nitrided reference powders of TiO, 9.3 wt %, and TiO_2, 17.1 wt %. On the basis of the apparent similarities, it is tempting to say that the 1000 °C nitridation of aerosols from the aqueous systems provides products similar to those of the nitridation of pure TiO, i.e., mainly oxynitrides. At the same time, relevant nitridation of aerosols from the methanol solution systems and from neat titanium(IV) *i*-propoxide parallels to some extent the nitridation of pure TiO_2 by showing similar and much-higher O content levels that can be linked to less-efficient reactions and significant quantities of unreacted TiO_2.

The nitriding pyrolyses at 1100 and 1200 °C provide products in the aqueous systems with a residual O content below 2 wt %. Similar pyrolyses of aerosols in the methanol-based and neat titanium(IV) *i*-propoxide systems result in products with slightly higher O content in the range 2.3−2.8 wt %. At this point, any similarities of these systems with the reference titanium oxide compounds appear to end because much-higher O content levels are observed in the related products from the latter. The highly crystalline character of the reference oxides at some point slows down the progress of nitridation, in contrast to all solvent-based systems with the likely nanosized formed oxides of increased reactivity.

The densities of the pyrolyzed aerosols have been anticipated to become higher with increased pyrolysis temperatures and, in many cases, that is what is determined. This trend is

Table 4. Oxygen Content and Helium Density of the Powders (n/d − Not Determined; sn/a − Sample Not Available)

pyrolysis temperature (°C)	oxygen content (wt %)	helium density d_{He} (g/cm^3)	pyrolysis temperature (°C)	oxygen content (wt %)	helium density d_{He} (g/cm^3)
	$Ti(NO_3)_4/H_2O/NH_3$			$Ti(O-i-C_3H_7)_4/CH_3OH/NH_3$	
1000	7.8	4.9	1000	20.5	4.1
1100	1.7	5.2	1100	2.6	5.2
1200	1.8	5.2	1200	n/d	4.9
	$TiCl_4/H_2O/NH_3$			Neat $Ti(O-i-C_3H_7)_4/NH_3$	
1000	3.5	5.0	1000	13.4	4.6
1100	1.3	5.2	1100	2.8	5.1
1200	n/d[a]	5.2	1200	2.3	5.25
	$Ti(OCH_3)_4/CH_3OH/NH_3$			Reference TiO/NH_3 (theor. O content in oxide, 25.05 wt %)	
1000	23.7	4.0	1000	9.3	4.7
1100	2.7	5.26	1100	10.8	4.9
1200	n/d[a]	4.9	1200	n/d	5.0
	$Ti(OC_2H_5)_4/CH_3OH/NH_3$			Reference TiO_2/NH_3 (theor. O content in oxide, 40.06 wt %)	
1000	22.2	4.0	1000	17.1	4.7
1100	2.3	5.1	1100	sn/a	sn/a
1200	2.5	4.8	1200	6.5	5.0

caused by the expected replacement of the intermediate titanium oxides of lower densities, i.e., $d(TiO_2/\text{rutile}) = 4.26$ g/cm^3, $d(TiO_2/\text{anatase}) = 3.84$ g/cm^3, $d(TiO) = 4.95$ g/cm^3, by the target titanium nitride, with $d(TiN) = 5.24$ g/cm^3. Densities of the transient oxynitride are expected to be between the values for TiO and TiN, generally higher than 5 g/cm^3. There is also a similar trend, as already encountered when discussing the average crystallite size changes from XRD (vide intra), in that most of the density increases take place up to the pyrolysis at 1100 °C (compare the 1000 and 1100 °C cases). Many density values for the aerosols pyrolyzed at 1100 °C and higher are equal or very close to the density of TiN.

The BET surface areas range from 4−7 m^2/g in the aqueous solution-derived powders to 20−30 m^2/g in the methanol solution-derived powders after the 1100 °C nitriding pyrolysis. These rather low values are indicative of mostly meso- and macroporosity.

4. Summary

A convenient two-stage aerosol-assisted processing technique is shown for a range of precursor/solvent systems, yielding nanocrystalline titanium oxynitrides and/or titanium nitride powders with spherical particle morphology. The characterization data strongly support the conclusion that most of the nanopowders prepared in the 1100−1200 °C range are composed of titanium nitride TiN with particle surfaces passivated with secondary titanium oxide TiO_2 and minimal, if any, titanium oxynitride TiO_xN_y. On the other hand, some of the powders prepared by pyrolysis at 1000 and 1100 °C contain the cubic phase of titanium oxynitride.

Under the applied conditions, the aqueous aerosol systems appear to be more prone to nitridation compared with the methanol solvent and neat titanium alkoxide systems, resulting in TiN powders containing the least residual oxygen. After nitriding pyrolyses at 1100−1200 °C, the aqueous system yields TiN powders with a residual oxygen content below 2 wt %, average crystallite size of 37−43 nm, and helium density of approximately 5.2 g/cm^3. At a lower pyrolysis temperature of 1000 °C, powders of cubic oxynitrides TiO_xN_y ($a = 4.222-4.227$ Å) with an O content of 3.5−7.8 wt %, average crystallite size of 26−29 nm, and density in the range 4.9−5.0 g/cm^3 are produced. The powders display spherical morphology not much affected by the conditions of the second nitridation/pyrolysis stage.

The methanol solution and neat titanium alkoxide aerosol systems yield high-quality TiN powders after the pyrolysis at 1100 °C. The processing results in a residual oxygen content in the range 2.3−2.7 wt %, average crystallite size of 32−35 nm, and helium density in the range 5.1−5.2 g/cm^3. The pyrolysis at 1000 °C yields in these precursor systems mostly mixtures of cubic oxynitrides and TiO_2. The initially spherical morphology of the methanol aerosols is significantly altered after the nitriding/pyrolysis stage to result in mostly empty-shelled spheres. Products prepared from neat $Ti(O-i-C_3H_7)_4$ show less tendency toward the spheroidal morphology.

There is analytical evidence that the carbothermal reduction/nitridation mechanism plays a significant role in the methanol solvent and neat titanium alkoxide systems during the aerosol-generation stage. Despite the clear improvement in the progress of the initial nitridation, the final products after the additional pyrolysis contain more oxygen than the carbon-deprived powders from the aqueous systems.

The most-obvious consequence of the utilization of methanol solutions or neat precursor are different particle morphologies of the resulting powders compared to those of the aqueous solution systems.

Acknowledgment. J.F.J. wishes to acknowledge the financial support of the Ministry of Education and Science (Poland), Grant 3 T08D 043 26. R.T.P. acknowledges support from the National Science Foundation, Grant CHE-9983205, which includes support for the international United States−Poland collaboration.

Note Added after ASAP Publication

A value in Table 4 has been changed from the first published version of this paper.

CM060522Z